S.M. Adler-Golden, S.C. Richtsmeier, A. Berk and J.W. Duff, *Fast Monte Carlo-assisted Simulation of Cloudy Earth Backgrounds*, SPIE Optical Engineering, Vol. TBD, (2012).

http://dx.doi.org/DOI# TBD

See article below.

Fast Monte Carlo-assisted simulation of cloudy earth backgrounds

Steven Adler-Golden*, Steven C. Richtsmeier, Alexander Berk and James W. Duff
Spectral Sciences, Inc., 4 Fourth Avenue, Burlington, MA 01803-3304

ABSTRACT

A calculation method has been developed for rapidly synthesizing radiometrically accurate ultraviolet through long-wavelength infrared spectral imagery of the Earth for arbitrary locations and cloud fields. The method combines cloud-free surface reflectance imagery with cloud radiance images calculated from a first-principles 3-D radiation transport model. The MCScene Monte Carlo code [1-4] is used to build a cloud image library; a data fusion method is incorporated to speed convergence. The surface and cloud images are combined with an upper atmospheric description with the aid of solar and thermal radiation transport equations that account for atmospheric inhomogeneity. The method enables a wide variety of sensor and sun locations, cloud fields, and surfaces to be combined on-the-fly, and provides hyperspectral wavelength resolution with minimal computational effort. The simulations agree very well with much more time-consuming direct Monte Carlo calculations of the same scene.

Keywords: background, scene, simulation, Monte Carlo, clouds, hyperspectral, multispectral

1. INTRODUCTION

The design of optical remote sensing systems requires good estimates of the anticipated radiance levels and their spectral and spatial distributions. In particular, there is a need for software that can rapidly generate a wide, representative variety of radiometrically accurate images of the earth's atmosphere and surface at arbitrary optical wavelengths, ranging from the ultraviolet (UV) to the long-wavelength infrared (LWIR), as viewed from aircraft and spacecraft.

The biggest challenge is the quantitative modeling of cloud fields and their effects, which require calculations with a 3-D radiation transport (RT) code. Such calculations are computationally intensive, making them prohibitive for on-the-fly use and limiting the ability to assemble comprehensive scene libraries. The input variables that specify a scene are numerous, and include surface properties, which are geographically and seasonally dependent, observer line-of-sight variables, sun illumination angles, wavelength, atmosphere model and cloud type and coverage. An image library that fully covers the scenarios of interest might require around 10^4 monochromatic images, each of which might take an hour or more to compute on a PC processor with a 3-D Monte Carlo RT code such as MCScene [1-4].

This paper describes a practical approach for rapidly generating arbitrary earth background scenes with the wavelength and spatial resolution and coverage of typical hyperspectral and multispectral sensors. The key is to use first-principles RT equations to decompose the image radiance into separate components that depend on only a small number of input variables, thereby reducing the required calculations by orders of magnitude. Pre-calculated cloud field databases are combined with separate surface and upper atmospheric descriptions to build the desired scene. Separate RT models are used for solar and thermal radiation sources. The models generalize standard equations used for atmospheric compensation in clear sky conditions [5] to the case of an inhomogeneous 3-D atmosphere. The cloud field images are calculated by MCScene using a voxelized cloud model. A local correlation-based data fusion method is used to suppress Monte Carlo "photon" noise, dramatically speeding the convergence of the calculations and enabling assembly of an extensive cloud image database in reasonable time. In addition, the observed low spectral dimensionality of the cloud field database allows the use of sparse pixel sampling to extend the simulations from the multispectral domain (several to tens of bands) to the hyperspectral domain (hundreds of bands) with little or no additional computational effort.

The organization of this paper is as follows. Section 2 presents the radiation transport models for above-cloud views and outlines the MCScene cloud field calculations that provide the model inputs. Section 3 describes the noise reduction and sparse sampling methods used to reduce computation time. Section 4 presents example scene simulations and a comparison with an "exact" direct Monte Carlo simulation.

*adlergolden@spectral.com; phone 1 781 273-4770; fax 1 781 270-1161; www.spectral.com

2. RADIATION TRANSPORT MODELING

For the present we consider views of the ground from above the cloud tops. The key elements of the RT model are:

- Partitioning the radiance into contributions from a horizontally uniform upper atmosphere above the cloud tops, a heterogeneous atmosphere below the cloud tops, and the nominally flat earth surface (Figure 1);
- A 3-D radiance model for the lower atmosphere that utilizes spatially dependent optical properties;
- Methods for deriving the spatially dependent optical properties from 3-D RT calculations with uniform, spectrally flat surfaces.

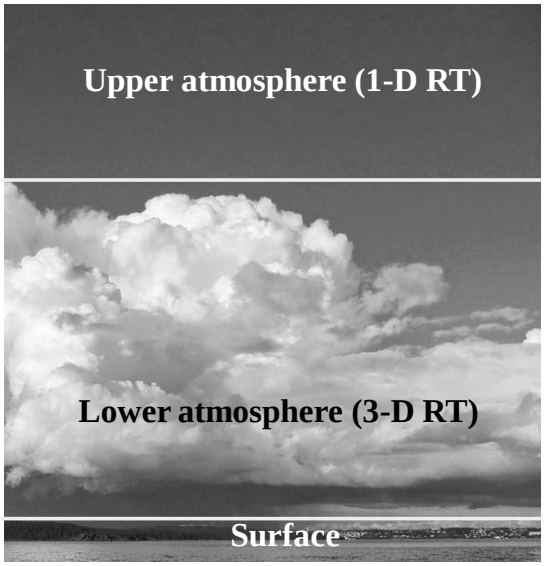

Figure 1. Partitioning of the scene into surface and atmospheric domains.

We note that the boundary altitude between the upper atmosphere, modeled with 1-D RT code, and the lower atmosphere, modeled with 3-D RT, is allowed to vary with the cloud field.

2.1 Upper/lower atmosphere radiance partitioning

Partitioning the observed radiance into upper and lower atmospheric components allows the time-consuming lower atmosphere calculations to be re-used for different sensor altitudes; the path from the cloud top to the sensor, located at altitude h, is modeled with a fast 1-D RT calculation. Let L_c denote the radiance at the *c*loud-top altitude, $t_{cd}(h)$ the *d*irect transmittance between the cloud-top altitude and the sensor, $t_{ci}(h)$ the *i*ndirect (diffuse) transmittance between the cloud-top altitude and the sensor, and $S(h)$ the path radiance between the cloud-top, z, and sensor altitudes. All of these quantities are both spatially and spectrally dependent. The radiance observed at the sensor may then be written as

$$L(h) = L_c\, t_{cd}(h) + \langle L_c \rangle\, t_{ci}(h) + S(h) \qquad \textbf{(1)}$$

L_c is computed as described in the following sections. The remaining quantities may be computed using an RT code for horizontally uniform atmospheres such as MODTRAN®[1] [6]. $\langle L_c \rangle$ in the second term denotes a spatially averaged image derived by convolving L_c with a point-spread function (PSF) describing the relative contributions from different parts in the scene to the diffusely transmitted radiance. The only significant contributor to this term is Rayleigh scattering. A satisfactory PSF may be obtained from the single-scattering limit, i.e., deriving the PSF from the Rayleigh scattering phase function [7]. The remainder of this paper concerns the calculation of L_c.

[1] MODTRAN computer software is a registered trademark owned by the United States Government as represented by the Secretary of the Air Force.

2.2 Radiance at the cloud-top altitude: solar component

The equation for the solar radiation component of L_c, like Eq. (1), contains directly transmitted, diffusely transmitted and scattered radiance contributions, with the diffusely transmitted contribution containing a spatial convolution. It is instructive to start with the special case of a horizontally uniform atmosphere and a Lambertian surface, where the radiance may be written as

$$L = a + b\,(t_d\,r + t_i\,\langle r\rangle)/(1-\langle r\rangle\sigma) \qquad \textbf{(2)}$$

Here a is the scattered path radiance term, b is the total solar flux transmitted to the ground, t_d is the effective direct transmittance between the ground and the sensor, t_i is the effective diffuse transmittance between the ground and the sensor, σ is the atmospheric spherical albedo, r is the surface reflectance at the imaged pixel, and $\langle r\rangle$ denotes a spatially averaged surface reflectance derived by convolving r with a PSF. All quantities in Eq. (2) are implicitly wavelength dependent, and r is spatially dependent. To model non-monochromatic in-band radiance, which does not obey Beer's law strictly, "effective" transmittance is defined as the ratio of transmittances along the total sun-ground-sensor and sun-ground paths.

The derivation of Eq. (2) [8] presumes spatial uniformity of illumination, transmittance and scattering, which then factor out of PSF convolutions. Including spatially dependent scattering, illumination, and transmittance due to clouds, but retaining a scene-average σ, a re-derivation yields the equation for L_c:

$$L_c = a + t_d\,[b + \langle rb\rangle\sigma/(1-\langle r\rangle\sigma)]\,r + t_i\langle[b + \langle rb\rangle\sigma/(1-\langle r\rangle\sigma)]\,r\rangle \qquad \textbf{(3)}$$

In cloudy scenes t_i is dominated by the cloud diffuse transmittance, which arises from various orders of scattering, each with its own PSF, making the net PSF spatially variable. Convolution with a spatially dependent PSF is in general quite computationally intensive. Fortunately, the dependence of the results on the PSF shape is found to be mild. Therefore we can approximate the PSF with a simple blend of single-scattering and multiple-scattering PSF convolutions, the proportions being based on the line-of-sight (LOS) optical depth (OD) at each pixel. For simplicity we take the multiple-scattering PSF to be proportional to the view factor between area elements of the ground and a surface located at the cloud center altitude; this represents the optically thick, physically thin limit of a non-absorbing uniform cloud.

2.3 Radiance at the cloud-top altitude: thermal component

The equation for the thermally emitted component of L_c (i.e., radiation not originating from the sun) contains path radiance and ground-reflected illumination terms, as in Eq. (3), plus direct and diffusely transmitted ground emission. The ground is specified by surface temperatures T as well as reflectances. Since even a cloudy atmosphere is essentially non-reflective at thermal wavelengths, the spherical albedo may be neglected. The ground thermal source is the product of its emissivity (1-r) and the Planck function $B(T)$. Therefore the thermal radiance at the cloud top altitude is given by

$$L_c = a + t_d\,rb + t_i\langle rb\rangle + f_d\,B(T)(1-r) + f_i\langle B(T)(1-r)\rangle \qquad \textbf{(4)}$$

Here the a term arises from thermal emission rather than scattering. We denote f_d and f_i as respectively the direct and diffuse transmittances of the ground emission up to the cloud top. In the monochromatic limit these are identical to the transmittances t_d and t_i, which pertain to the atmospheric downwelling radiance. However, when applying Eq. (4) to in-band quantities these sets of transmittances differ, because the spectral fine structure in the atmospheric transmission interacts differently with the spectrally correlated atmospheric illumination spectrum than with the much smoother ground emission spectrum.

2.4 Derivation of radiation transport quantities from MCScene

The Eq. (3) quantities are derived from MCScene calculations performed with a small set of uniform surface reflectances. An analogous derivation of RT quantities is used in the FLAASH atmospheric compensation code [7], where the RT model is MODTRAN®. Here the RT quantities are defined as 2-D maps (images) rather than single values. The MCScene calculations are performed for each desired wavelength, 3-D cloud field, model atmosphere, and combination of solar and viewing geometries.

One set of MCScene radiance images, for r=0.5 and 1, is calculated with the downlooking sensor placed just above the ground, thereby eliminating a and setting the transmittances equal to 1 in Eq. (3). Scene-averaging the two images leads to a pair of equations in σ and the scene-average b, which are solved for σ. The derived spherical albedo is used with Eq. (3) and the r=1 image to derive the b image. A second set of MCScene calculations is run for r=0 and 1 with the

sensor at the cloud-top altitude. The former yields a, while the latter yields t_i when t_d (a separate MCScene output) and the previously determined quantities are inserted into Eq. (3).

We note that the r=1 cloud-top view depends on both the viewing and solar angles, so at first glance its calculation appears to be necessary for each angle combination. However, this view is used only to derive t_i, which is independent of the sun angle. We find some dependence in practice; calculations of t_i with a low sun tend to be less credible, perhaps because of greater shadowing.

For thermal radiance modeling, the Eq. (4) quantities may be derived from four MCScene calculations. Two are for r=0 and r=1 from the cloud top with a cold (T=0) ground; one is for r=0 from the cloud top with a warm (e.g., ambient temperature) ground, and one is for r=1 from just above a cold ground. The solar angle is irrelevant in these calculations.

The remainder of this paper will focus on the solar wavelength region.

3. COMPUTATION PROCEDURE

3.1 Photon noise suppression

The main limiting factor in the MCScene calculation accuracy is statistical noise, which scales inversely with the square root of the number of Monte Carlo "photons". A clean-looking MCScene image (signal to noise of tens to 100) requires ~10^4 photons/pixel, which for a 500x500-pixel cloud field requires ~10 hours of computations on our dedicated multiprocessor system. However, we have found that for a spatial resolution of tens of meters comparably accurate results can be obtained with only 100 photons/pixel by fusing the output with cloud OD images. The fusion method involves spatial smoothing followed by insertion of high-resolution structure from a "reference" image using a local linear regression algorithm [9]. We have previously used a related method for MCScene image enhancement in which the reference image is surface reflectance [10]. For the views from ground level, an appropriate reference image for solar wavelength calculations is the solar LOS direct transmittance, exp(-OD), which renders the cloud shadows. For the a image, *i.e.*, r = 0, the reference is the sensor LOS OD, while for the r=1 image at the cloud top the reference is an analytical approximation to Eq. (2) that uses both sensor and sun LOS ODs.

3.2 Hyperspectral sparse sampling

When the MCScene cloud field calculations are performed for hundreds of narrow wavelength bands and a principal component analysis is performed, the spectral dimensionality of the image stack is found to be very low, around 2 to 3. This implies that the image at any arbitrary wavelength can be reconstructed from linear combinations of images at just a few wavelengths. We have found that the combination coefficients and a constant term can be derived via linear regression from 1000 photon/pixel spectral calculations for a few hundred pixels covering the sensor and sun LOS OD ranges. In particular, we have found that satisfactory cloud field images can be obtained throughout the solar wavelength region at hyperspectral resolution using full image calculations performed at only two wavelengths, 1.65 μm and 2.1 μm.

3.3 Cloud field models

We have employed two types of cloud models in our simulations to date. The numerical Cloud Scene Simulation Model (CSSM) developed by Cianciolo and Raffensberger [11] provides semi-empirical, time-dependent voxelized 3-D descriptions for a variety of cloud field types. We used the model to generate cumulus, altostratus and cirrus cloud fields at 20 m spatial resolution. The CSSM specifies the liquid water content in each cloud-containing atmospheric voxel, but for the simulations reported here we specified a fixed water content, and hence a fixed 550 nm OD, in all cloud voxels.

For a more realistic appearance we have also derived cloud fields from imagery, using Landsat-7 measurements over water with the CSSM as a guide. Very briefly, the procedure involves the following steps:

- Estimating an altitude range for the cloud tops based on a CSSM calculation;
- Estimating a cloud top altitude for each cloudy pixel by linearly mapping the Landsat-7 LWIR brightness temperature image onto the cloud top altitude range, consistent with the assumption of a constant atmospheric lapse rate;

- Estimating a cloud bottom altitude for each cloudy pixel using a CSSM-based relationship between cloud top and bottom altitudes;
- Choosing a voxel OD that reasonably models the Landsat-7 cloud brightnesses and shadow depths in a visible scene simulation.

MCScene uses the cloud model databases in MODTRAN® to assign a phase function and extinction and scattering cross sections to the cloud voxels. A standard MODTRAN® model atmosphere, which defines the upper atmosphere and overlays the cloud field in the lower atmosphere, is chosen to complete the specification of all optical properties required for MCScene.

4. EXAMPLE RESULTS AND CONCLUSIONS

Our initial work focused on developing and validating the scene-building procedure based on Eq. (3). Then we assembled a library of results from 100 photon/pixel MCScene calculations at 20 m pixel resolution for several different cloud types, viewing and sun elevation angles and relative azimuth angles. The library data were combined with multispectral or hyperspectral surface reflectance images to generate scenes viewed from the cloud tops. A few example scenes are presented here. The images were generated from apparent spectral reflectance values (spectral radiance divided by the solar function) using ENVI (Environment for Visualizing Images) software.

Figure 2 illustrates the simulation of a nadir view of Sacramento, CA for the 1.65 μm band with a CSSM altostratus cloud field. The sun is low, 15° above the horizon, and the observer is at the cloud-top altitude of 3 km. The library 100 photon/pixel MCScene cloud field simulation for r=1 is at top left. The result after noise suppression is at top right, and the noise-suppressed simulation for r=0 is at lower left. The scene at lower right was generated by combining the cloud field calculations with a Landsat-7 image converted to reflectance using FLAASH [6,7].

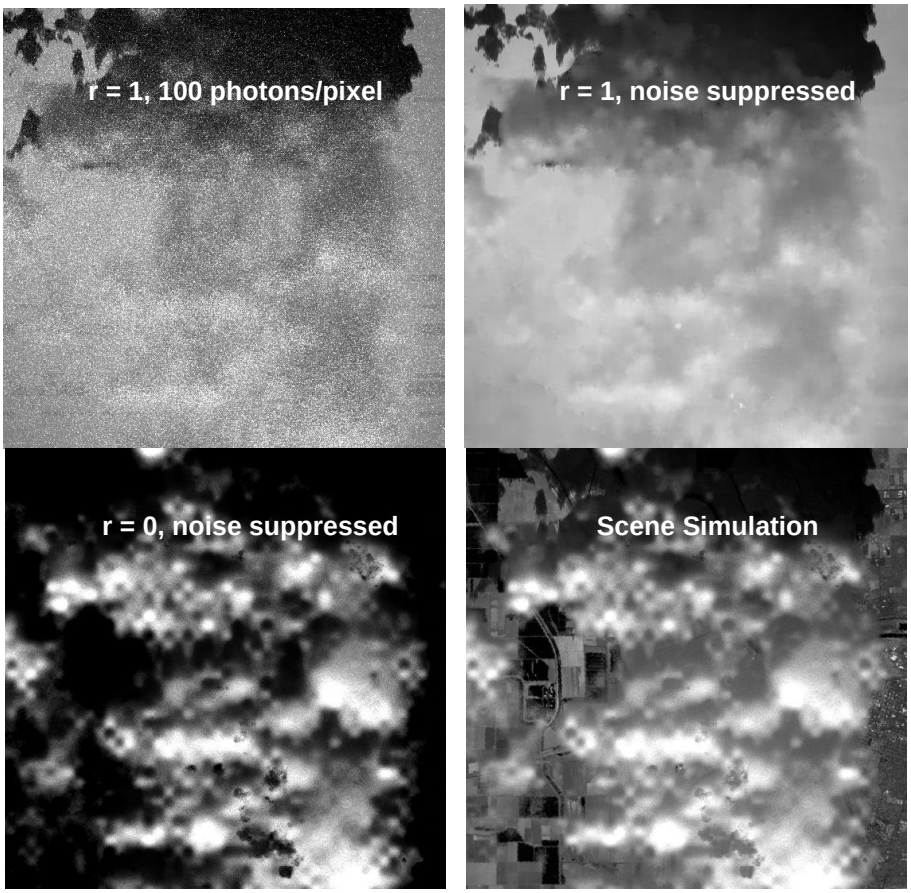

Figure 2. Simulation of a cloudy scene for Sacramento, CA at 1.65 μm.

A direct MCScene "truth" calculation of the above scene was then made using 10,000 photons/pixel, and the results were compared. Visually the two images are almost identical, the main difference being the presence of a small amount of Monte Carlo noise in the "truth". The RMS difference is very low, 0.018 apparent reflectance units, and this drops to 0.013 with 3x3-pixel smoothing, which suppresses Monte Carlo noise.

Figure 3 at left shows a simulated nadir view of Tampa Bay near Bradenton, FL in visible true color (grayscale in the hardcopy paper). This scene combines a FLAASH-processed AVIRIS image [12] with a Landsat-derived cumulus cloud field. The sun elevation angle is 45°. The original Landsat scene, taken over the Pacific Ocean with a slightly higher sun angle, is shown at right. Modest differences in cloud shading and different locations of the cloud cast shadows result from the angle difference, and the brightest Landsat clouds are affected by sensor saturation. Nonetheless, the simulation is seen to represent the original cloud field with good fidelity.

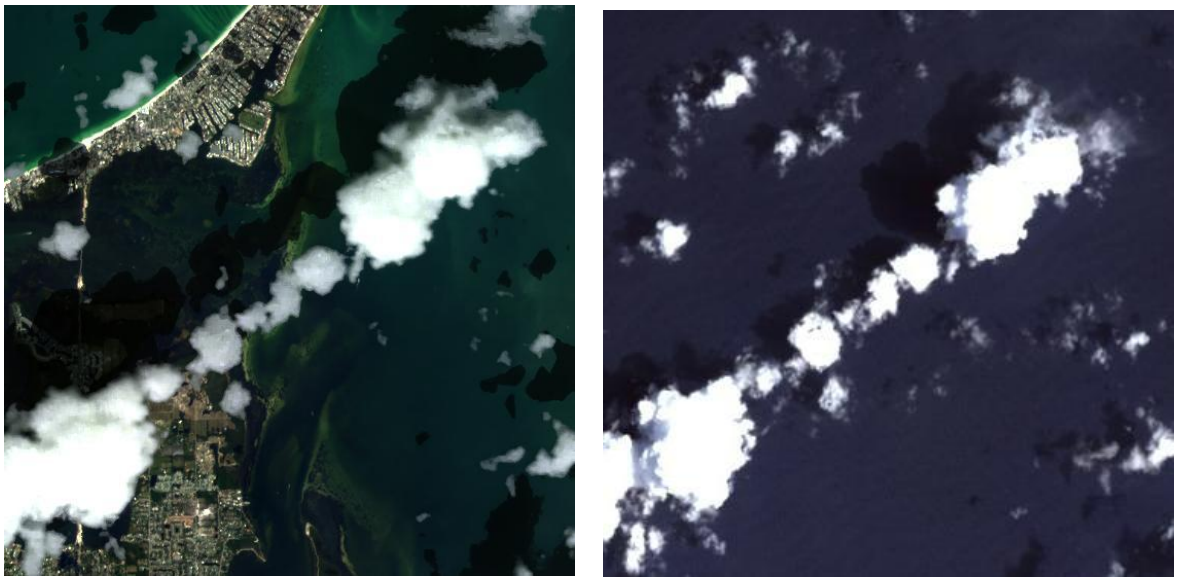

Figure 3. At left, synthetic visible (red-green-blue) image of Tampa Bay, FL; at right, original cloud-containing Landsat image over the Pacific Ocean.

Figures 4a-d show some simulated slant views of Tampa Bay looking towards the sun (180° relative azimuth angle). Since water is not well represented by the model's Lambertian surface assumption, an approximate treatment of water glint is included. Figures 4a-c use the same cloud field as in Figure 3. A low sun elevation angle of 15° yields a very high contrast scene, with large cloud forward scattering, a very dim surface, and yellowish lighting. Figures 4b-d use a sun elevation angle of 45°. In Figure 4c, constructed from infrared bands, there is higher contrast than in the visible due to lower aerosol scattering and darker water at these longer wavelengths. Finally, Figure 4d shows a variant of the Figure 4c scene with a Landsat-derived cirrus cloud field.

The current results indicate that this fast cloudy scene simulation method should have more than enough accuracy and wavelength versatility to address a wide range of system design and evaluation applications. In addition, it may be useful for developing algorithms for remote sensing of surface, cloud and atmospheric properties from multispectral or hyperspectral imagery under cloudy conditions. Further work is underway to exercise the method over a wider variety of viewing geometries, wavelengths, and atmospheric conditions, and to validate the model for thermal emission.

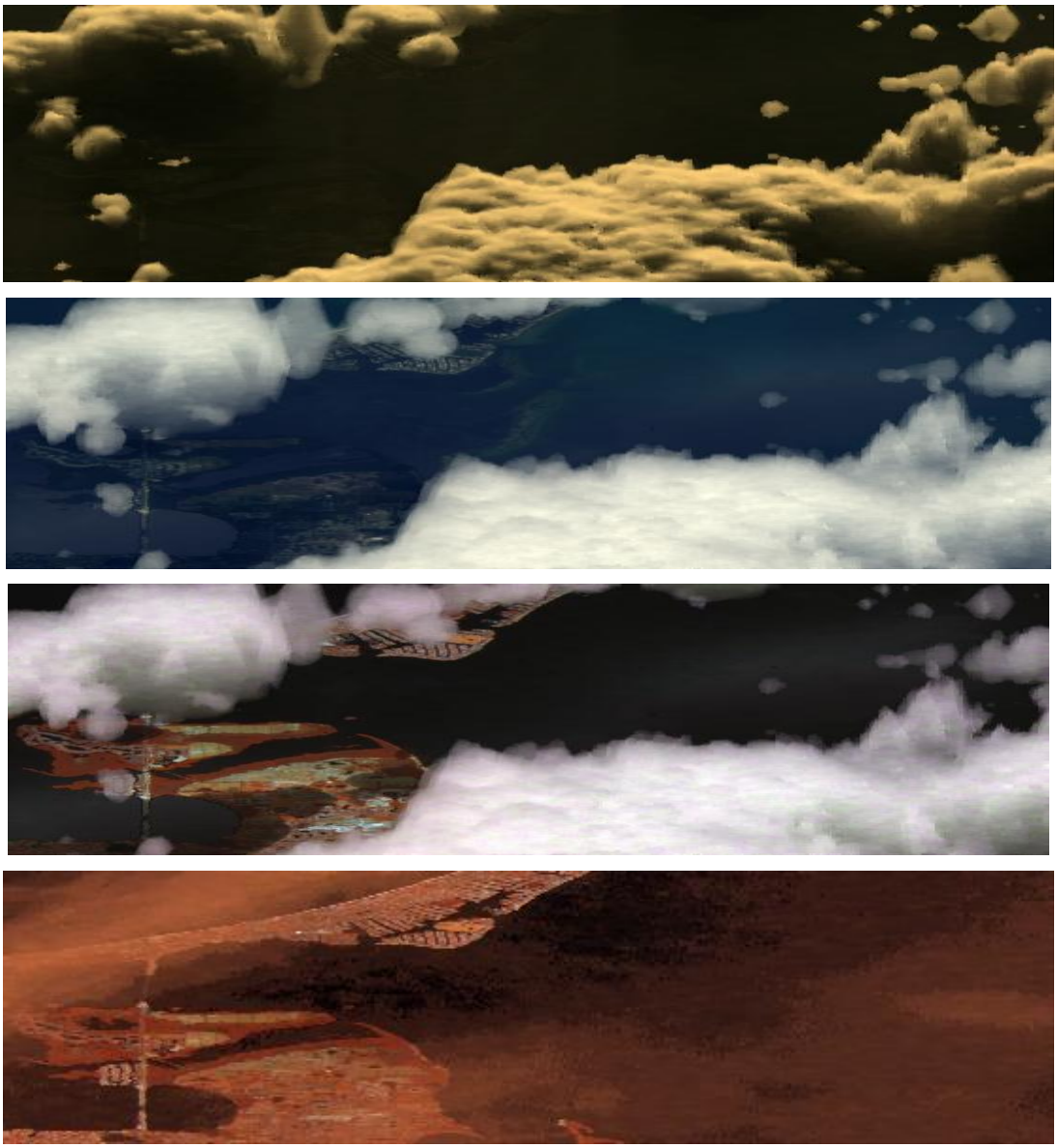

Figures 4a-d. Synthetic images of Tampa Bay for a 15° view elevation angle and a 180° relative azimuth angle between the observer and the sun. From top to bottom, (a) visible (red-green-blue) wavelengths, sun elevation angle = 15°, Figure 3 cloud field; (b) as in 4a but with sun elevation angle = 45°; (c) as in 4b but in the infrared (R,G,B = 1.04, 1.64, 2.09 μm); (d) as in 4c but with a cirrus cloud field.

5. ACKNOWLEDGMENTS

The authors wish to acknowledge Spectral Sciences, Inc. for support under an internal research and development grant. The authors also wish to acknowledge Wellesley Pereira and other members of AFRL/RVBYM for their continuing support and technical discussions on the validation of MCScene code.

6. REFERENCES

[1] Adler-Golden, S. , S.C. Richtsmeier, A. Berk and J.W. Duff, "Fast Monte Carlo-Assisted Simulation of Hyperspectral Earth Backgrounds," Third Annual WHISPERS Conference, Lisbon, Portugal, 6-9 June (2011).

[2] Sundberg, R., S. Richtsmeier, and R. Haren, "Monte Carlo-Based Hyperspectral Scene Simulation," Second Annual WHISPERS Conference, Reykjavik, Iceland, 14-16 June (2010).

[3] Richtsmeier, S., R. Sundberg, R. Haren, and F.O. Clark, "Fast Monte Carlo full spectrum scene simulation," Proc. SPIE 6233, (2006)

[4] Sundberg, R.L., S. Richtsmeier, and R. Haren, " Improved Full Spectrum Cloudy Scene Simulation," Proc. SPIE 7107, Cardiff, Wales, (2008).

[5] Matthew, M. W., S. M. Adler-Golden, A. Berk, G. Felde, G. P. Anderson, D. Gorodetzky, S. Paswaters and M. Shippert, "Atmospheric Correction of Spectral Imagery: Evaluation of the FLAASH Algorithm with AVIRIS Data," SPIE Proceeding, Algorithms and Technologies for Multispectral, Hyperspectral, and Ultraspectral Imagery IX (2003).

[6] Berk, A., L.S. Bernstein, G.P. Anderson, P.K. Acharya, D.C. Robertson, J.H. Chetwynd and S.M. Adler-Golden, "MODTRAN® Cloud and Multiple Scattering Upgrades with Application to AVIRIS," Remote Sens. Environ. 65:367-375 (1998).

[7] Adler-Golden, S.M., M.W. Matthew, A. Berk, M.J. Fox, J. Lee, and A.J. Ratkowski, "Improvements in Aerosol Retrieval for Atmospheric Correction," IEEE International Geoscience & Remote Sensing Symposium, Boston, MA, July 6-11 (2008).

[8] Vermote, E., D. Tanre, J.L. Deuze, M. Herman, and J.J. Morcrette, "Second Simulation of the Satellite Signal in the Solar Spectrum (6S)," 6S User Guide Version 6.0, NASA-GSFC, Greenbelt, Maryland, 134 pages (1994).

[9] Tom, V.T. and M.J. Carlotto, "Adaptive least-squares technique for multi-band image enhancement," Proc. ICASSP International Conference on Acoustics, Speech and Signal Processing, Tampa, Florida, 26-29 March, pp. 704-707 (1985).

[10] Adler-Golden, S., D. C. Robertson, S. C. Richtsmeier, and A. J. Ratkowski, "Cloud Effects in Hyperspectral Imagery from First-Principles Scene Simulations," Algorithms and Technologies for Multispectral, Hyperspectral, and Ultraspectral Imagery XV, Edited by Shen, S.; Lewis, P., Proc. SPIE, 7334, pp. 73340Z-73340Z-12 (2009).

[11] Cianciolo, M.E. and M.E. Raffensberger, "Atmospheric Scene Simulation Modeling and Visualization (AMV)," Cloud Scene Simulation Model User's Guide, TIM-07169-2, TASC, Reading, MA (1996).

[12] Adler-Golden, S.M., P.K. Acharya, A. Berk, M.W. Matthew and D. Gorodetzky, "Remote Bathymetry of the Littoral Zone From AVIRIS, LASH, and QuickBird Imagery," *IEEE Trans. Geosci. Remote Sens*., 435, 337-347 (2005).